

X-ray spectroscopy of the weak-lined T Tauri star HD 283572

F. Favata¹, G. Micela², and S. Sciortino²

¹ Astrophysics Division – Space Science Department of ESA, ESTEC, Postbus 299, 2200 AG Noordwijk, The Netherlands

² Osservatorio Astronomico di Palermo, Piazza del Parlamento 1, I-90134 Palermo, Italy

Received 2 April 1998 / Accepted 3 June 1998

Abstract. We have analyzed the existing X-ray spectroscopic data for the Weak-Line T Tauri star (WTTS) HD 283572, from the ROSAT, ASCA and SAX satellites. All the data sets are well fit with an absorbed two-temperature model based on collisional ionization equilibrium. Together with the *Einstein* data discussed in the literature, these data sets afford a 16.5 years time span, allowing to study the short- and long-term spectroscopic and photometric variability characteristics of the X-ray emission from WTT stars. The X-ray luminosity of HD 283572 appears to vary by factors of $\simeq 2$ on time scales of tens of kiloseconds, within a single observations, while its average X-ray luminosity has varied by a factor of $\simeq 2.5$ (peak-to-peak) along the 16.5 yr studied here. The SAX observation also shows evidence for a short flare, with an enhancement of the X-ray luminosity by a factor of $\simeq 4$.

Key words: stars: individual: HD 283572 – stars: late-type – stars: activity – stars: coronae – X-rays: stars

1. Introduction

Pre-main sequence (PMS) stars are well known luminous coronal soft X-ray sources, with high levels of X-ray emission observed both from Classical T-Tauri stars (CTTS), showing evidence for a circumstellar disk, and from Weak-line T-Tauri stars (WTTS), which have an age distribution overlapping with the one of CTTS but show no evidence for a disk.

The optically bright WTTS HD 283572 ($V = 9.3$) was discovered from its bright X-ray emission (Walter et al. 1987); it is a member of the Taurus-Auriga star-forming region, and its Hipparcos parallax ($\pi = 7.81 \pm 1.3$) implies a distance of 128 pc, with a 1σ confidence region extending from 110 to 154 pc. The implied evolutionary age using the Hipparcos parallax is $\simeq 3$ Myr, and the derived mass is $\simeq 2.2 M_{\odot}$ (Favata et al. 1998), with no significant changes with respect to previous estimates. Its characteristics are described in detail by Walter et al. (1987), who derived an MK spectral type of G5 IV, and a radius of $3.3 R_{\odot}$, at an assumed distance of 160 pc, which becomes

$2.7 R_{\odot}$ at the Hipparcos distance. The optically-derived absorbing column density is $A_v = 0.57$ (Strom et al. 1989), and the projected rotational velocity $v \sin(i)$ is $\simeq 100 \text{ km s}^{-1}$. The measured value of A_v is high for the measured distance to HD 283572, and is therefore likely not due to the intervening interstellar matter, but is rather local to the source, as can be expected for a very young star with other signs of circumstellar matter, such as IR excess. No direct measurements of its photospheric metal abundance are available in the literature; however, Padgett (1996) recently determined the photospheric Fe abundance in a group of pre-main sequence stars in the Taurus-Auriga region, showing that they have, within the measurement error, solar-like abundances. Thus, in the following we will assume solar photospheric abundances for HD 283572.

HD 283572 is a very luminous X-ray coronal source: from *Einstein* data Walter et al. (1987) derived a luminosity in the 0.1–4.1 keV band of $2 \times 10^{31} \text{ erg s}^{-1}$, at the upper end of the observed X-ray luminosities in single young active stars. This high X-ray luminosity, combined with its relative proximity to the Sun, makes HD 283572 a unique object, as it offers the opportunity of studying the spectral characteristics of the soft X-ray emission from a pre-main sequence star without a disk. Indeed, HD 283572 has been observed with most of the X-ray (and UV) telescopes flown to date, including the *Einstein*, EXOSAT, ROSAT and ASCA X-ray observatories and the IUE ultraviolet observatory. In the present paper we perform a combined study of the X-ray spectrum of HD 283572, using the data from the ROSAT, ASCA and SAX observatories. HD 283572 is perhaps the only known WTTS with a confirmed position above the main sequence (Favata et al. 1998) which is sufficiently bright in X-rays to make it possible to study in detail the X-ray spectrum with the available X-ray telescopes. Other nearby very young stars for which detailed spectroscopic studies are possible (such as AB Dor) appear to be, on the basis of their Hipparcos distance, much closer to (or onto) the main sequence and therefore in a different evolutionary state than HD 283572.

2. The *Einstein* and EXOSAT data

HD 283572 was first observed, in the X-rays, by the IPC instrument onboard the *Einstein* observatory, in sequences I3843 and I4507, both taken on Feb. 2, 1980, within a few hours of

Send offprint requests to: F. Favata

Correspondence to: ffavata@astro.estec.esa.nl

each other. In both cases HD 283572 was seen as a serendipitous source in the observation, the main targets being nearby classical T-Tauri stars. A spectroscopic analysis of the data for sequence I4507 was done by Schrijver et al. (1984)¹, who found that the IPC data are well fit by an isothermal optically thin plasma spectrum with a best-fit temperature of 1.12 keV and a best-fit absorbing column density of 10^{21} cm⁻². For the same data Walter et al. (1987) find that the X-ray luminosity in the 0.1–4.1 keV band, using a distance of 160 pc, is 2.0×10^{31} erg s⁻¹. The observation from sequence I3843 took place about 10 ks later, and according to Walter et al. (1987), there are no significant changes neither in the spectrum nor in the count rate between the two IPC data sets. The data from the IPC sequence I4507 were subsequently re-analyzed (using the REV1 processing, unlike the previous work which made use of the REV0 processing²) by Damiani et al. (1995), who derive an X-ray luminosity of 2.5×10^{31} erg s⁻¹ (at an assumed distance of 140 pc), or, rescaled to the Hipparcos-derived distance, 2.1×10^{31} erg s⁻¹. As shown later, the X-ray luminosity derived by the IPC observation is higher than any of the subsequently derived values. No mention of flaring activity is however made in the literature regarding the IPC data, thus we performed a temporal analysis of the original IPC data for both sequences, finding that the data (binned at 300 s intervals) are consistent with the source being constant, both within each single observation as well as across the two observations, with the null hypothesis of their variability rejected to a high degree of confidence. HD 283572 was also observed with the EXOSAT low-energy telescope, but was not detected, and the upper limit to its flux is, according to Walter et al. (1987), consistent with its X-ray luminosity at the time of the IPC observations.

3. Observations and data analysis

3.1. The data sets

We have retrieved the ROSAT, ASCA and SAX X-ray observations of HD 283572 from the respective public archives, making use of the HEASARC service for the ASCA and ROSAT data and of the SAX-SDC archive for the SAX observations. None of the data sets presented here has been previously discussed in the literature. The journal of the observations is shown in Tab. 1.

3.1.1. ROSAT observation

The ROSAT observation of HD 283572 took place from March 3 to March 6, 1993, with the PSPC-B detector. The effective exposure time was 5.45 ksec. The P.I. of the observation was F. Walter. The observation was executed in 5 short segments, spanning approximately three days of elapsed time.

The background-subtracted count-rate for the PSPC spectrum was 0.35 cts s⁻¹, for a total of 1.9 kcts in the spectrum

¹ where HD 283572 is referred to as SAO 76567.

² REV1-processed data feature improved gain correction, event screening and background rejection, thus ensuring significantly lower systematics. See Damiani et al. (1995) for details.

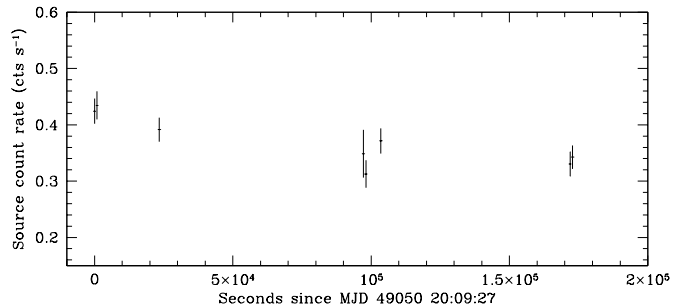


Fig. 1. The X-ray light-curve of HD 283572 in the 0.2–2.2 keV band during the ROSAT PSPC observations, binned in 900 s intervals.

Table 1. Journal of the observations. The *Einstein* IPC observation I4507 is also included for ease of comparison, although it was not analyzed here. The “live time” entry refers to the effective exposure time for the given observation, while the entry “elapsed time” refers to the total elapsed time from the beginning until the end of the observation.

Instrument	Date	Time (ks)	
		Live	Elapsed
<i>Einstein</i> IPC	2 Feb. 1980	3.2	8
PSPC-RASS		0.5	–
PSPC-ROSAT	3–6 Mar. 1993	5.5	175
ASCA-SIS	15 Sep. 1995	20.1	58
SAX-LECS	27 Sep. 1996	11.6	157
SAX-MECS	27 Sep. 1996	76.0	157

between 0.2 and 2.2 keV. The spectrum was rebinned to have at least 20 counts per rebinned channel. The light-curve of the PSPC observation, accumulated in bins of 900 s each, is shown in Fig. 1. The response matrix used for the spectral fitting is the one known as PSPCB_GAIN2_256.RSP, obtained from the HEASARC data archive (with a creation date of Feb. 2, 1993), and recommended for the analysis of on-axis sources.

HD 283572 was also detected in the ROSAT All Sky Survey (RASS), with a count rate of 0.317 cts s⁻¹, very similar to the one of the pointed observation.

3.1.2. ASCA observation

HD 283572 was observed by the ASCA satellite on Sep. 15, 1995, starting at 23 hr UT, for a total of 20.1 ks effective exposure time. The P.I. of the observation was F. Walter. We have analyzed the data from the SIS0 detector, which was taken in the BRIGHT mode and at HIGH bit-rate. The observation, as retrieved from the public archive, has been reduced with the FTOOLS package, version 4.0, which was used for the source counts extraction as well as for the generation of the response matrix. Source counts have been extracted from a circular region of 4.35 arcmin diameter. The resulting light-curve of the SIS observation, accumulated in 900 s bins, is shown in Fig. 2. The source spectrum was extracted from the same region as the

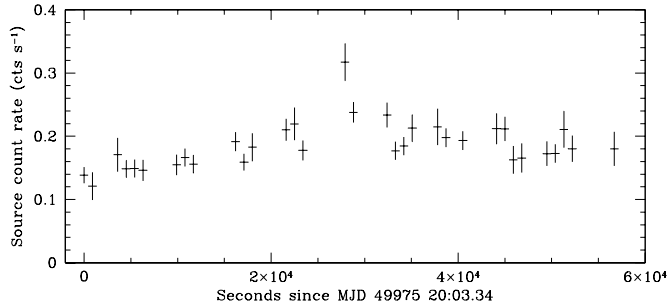


Fig. 2. The X-ray light-curve of HD 283572 in the 0.5–7.0 keV band during the ASCA observations, binned in 900 s intervals.

light curve, and the background was extracted from the same observation, using the whole field with the exclusion of a circular region of diameter 6.37 arcmin, also centered on the X-ray source. The background-subtracted count rate for the source is 0.163 cts s^{-1} , for a total of 3.2 kcts in the spectrum between 0.5 and 7.0 keV. The spectrum was rebinned to have at least 20 counts per rebinned channel. The response matrix for the ASCA observation was generated with the ASCAARF version 2.72 and SISRMG version 1.1 tools.

3.1.3. SAX observation

HD 283572 has been the first coronal source observed in the guest observer program with the SAX observatory. The SAX observatory features 4 co-aligned soft X-ray instruments, i.e. one LECS detector with a passband of 0.1–10. keV and three MECS detectors, with a passband of 1.5–10. keV. The P.I. of the observation was E. Covino, and the observation took place starting at 20:51 of 27 Sep. 1996. The observation covers $\simeq 150$ ks of elapsed time, with 76.0 ks effective observing time for the 3 MECS detectors and only 11.6 ks effective observing time for the LECS detector. The short LECS exposure is due to a combination of the intrinsically lower efficiency of the LECS detector (which is operated during Earth night only) and to the fact that the detector was apparently malfunctioning during the final part of the observation.

The SAX data (for both the LECS and the three MECS detectors) were processed through the SAXPIPE software, producing linearized event files, from which spectra and light curves were extracted using the XSELECT software.

The spectra were extracted with a diameter of 8.2 and 4.0 arcmin for the LECS and MECS data, respectively, while the background was extracted from regions of the same size and location as the source extraction region from the standard background files supplied by the SAX-SDC. Standard response matrices were used for the MECS spectra, while a matrix was computed ad hoc for the LECS spectrum using the LEMAT program. The source count rate are 0.085 and 0.098 cts s^{-1} in the LECS and in the three merged MECS detectors, respectively. Fig. 3 shows the merged light-curve of the 3 MECS detectors, binned at 900 s resolution.

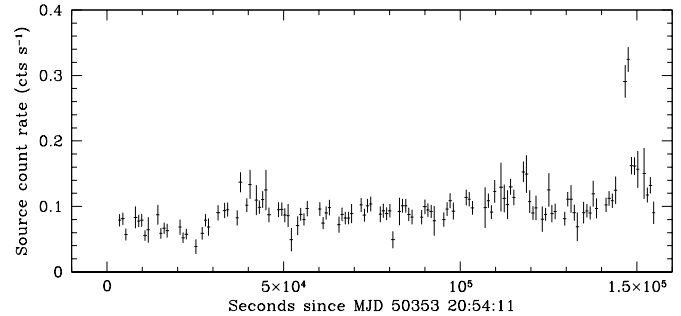


Fig. 3. The merged X-ray light-curve of HD 283572 as seen by the 3 MECS detectors, in the 1.5–10. keV band during the SAX observations. The data are binned in 900 s intervals.

3.2. The X-ray light curves

Both the ROSAT (Fig. 1) and the ASCA (Fig. 2) light curves show evidence for a modest level of variability, i.e. $\sim 60\%$, on time scales of the order of tens of kiloseconds. In addition, the SIS light-curve shows some evidence for more rapid and intense, flare-like variations in the segment between 25 and 35 ks from the beginning of the SIS observation.

A simple χ^2 test shows that the probability of the SIS lightcurve being constant is 1.6×10^{-3} , while a Kolmogorov-Smirnov (KS) test yields a probability of constancy of only 4.9×10^{-10} . For the PSPC light-curve the probabilities of constancy are 4.4×10^{-2} and 1.5×10^{-5} for the χ^2 and KS tests, respectively. In the case of the KS the test statistic is the maximum deviance between the observed and the expected distributions (in this case a constant), while the test statistic for the χ^2 test is a normalized average deviation. Thus, the KS test is more sensitive to short-lasting but significant deviations from constancy (i.e. flare-like events), while the χ^2 is more sensitive to, for example, slow trends in the data.

The SAX light curve (from the three merged MECS detectors, Fig. 3) shows the same type of continuous variability on time scales of tens of ks as seen in the ASCA and ROSAT data, but with a larger amplitude (approximately a factor of $\simeq 3$ peak-to-peak). In addition, the light curve shows evidence for a short-duration flare taking place toward the end of the observation, with amplitude a factor of $\simeq 4$ above the average quiescent emission level. Unfortunately the low count-rate of the source does not allow for a detailed spectroscopic analysis of the flare. Excluding the flare, the source shows a very low probability of being constant, with a χ^2 square test yielding a probability of constancy $< 10^{-5}$.

The optical light curve of HD 283572 has been observed to be modulated, with a period compatible with the projected equatorial rotational velocity of the star (i.e. its $v \sin i$), showing that the system is in a nearly equator-on position. The measured modulation period of the optical light curve is 1.548 d, with a modulation amplitude of $\simeq 0.1$ mag (Walter et al. 1987). Doppler imaging of HD 283572 shows that the light modulation is compatible with the presence of a large nearly-polar spot (Joncour et al. 1994). Thus, if the X-ray emission is due to magnetically-confined plasma, the emitting material could per-

haps be expected to be concentrated above the spot, where the magnetic field is likely to be higher. If such plasma were to lie sufficiently close to the photosphere (i.e. a compact corona), the X-ray light curve would show a modulation in antiphase with the optical light curve. The ASCA exposure is too short to establish whether the observed variation in X-ray emission level is indeed due to rotational modulation, covering less than half a rotational period for the star, as is (because of the coverage) the ROSAT observation. The SAX observation is longer, covering 1.1 rotational periods, but unfortunately still insufficient to perform rigorous statistical tests to search for modulation at the optically determined period. Visual inspection of the SAX light curve does not however show any evidence for strong modulation of the X-ray flux at the rotational period of the star.

3.3. Spectral fits

3.3.1. Spectral fitting, ASCA spectrum

The ASCA spectrum was fit with a two-temperature collisional equilibrium of ionization model, using the MEKAL plasma emission code (Mewe et al. 1995) as implemented in the XSPEC version 10.0 package, which was used for all the fits discussed here. Absorption by either interstellar gas or local material was included according to the Morrison & McCammon (1983) model, adding a WABS XSPEC component to the model spectrum. The absorbing column density and the global metallicity of the spectrum were both left as free parameters. The spectrum was fit in the region from 0.5 to 7.0 keV, with the higher bound being determined by the lack of counts at the higher energies. The best-fitting model has temperatures of 0.88 and 2.5 keV and abundance very close to solar (with the best-fit value at 0.90 times solar, and thus close to the assumed photospheric abundance). The ratio between the cool and the hot emission measure ratio is 0.23. The X-ray luminosity, calculated using the Hipparcos distance, is 1.0×10^{31} erg s⁻¹ in the 0.2–10. keV band (or $\simeq 20\%$ less in the 0.2–3.5 keV band, and thus a factor of 3.8 times lower than at the time of the *Einstein* observation), and the emission measures for the cool and hot components are 1.21×10^{53} cm⁻³ and 5.35×10^{53} cm⁻³. The best-fit column density is 1.4×10^{21} cm⁻², corresponding to an optical absorption $A_v = 0.9$. The optically derived value is lower, at $A_v = 0.57$, however the rather broad error bars for the ASCA-derived value are such that the confidence regions include the optically-derived value.

The fit (for this as well as for other cases discussed in the present paper) were performed using the weighing criterium of Gehrels (1986), appropriate for data following Poisson statistics. The resulting reduced χ^2 , at 0.81 over 71 degrees of freedom, is fully acceptable, corresponding to a 87% probability that the model is consistent with the data. The ASCA spectrum, together with the best-fit two-temperature MEKAL model is shown in Fig. 4.

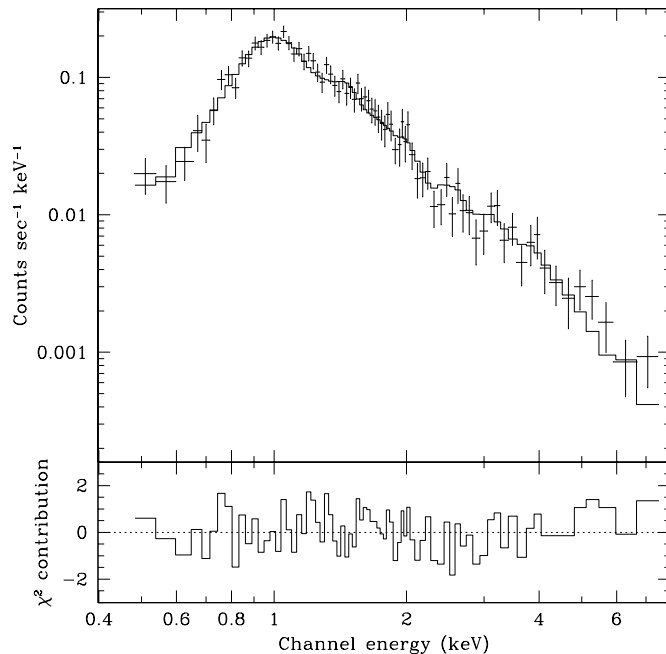


Fig. 4. Spectral fitting of the SIS data. The top panel shows the background-subtracted spectrum, rebinned to have at least 20 counts per (variable-size) bin, plotted together with the best-fit two-temperature MEKAL model with an absorbing column density, while the bottom panel shows the (signed) contribution of each bin to the total χ^2 .

3.3.2. Spectral fitting, PSPC spectrum

We have first verified that the PSPC spectrum is not satisfactorily fit with a single-temperature absorbed MEKAL model, with the resulting reduced χ^2 being in excess of 1.5. If the same model is used as for the ASCA spectrum, i.e. an absorbed two-temperature MEKAL model with a freely varying coronal abundance, a satisfactory fit is achieved. However, the PSPC data appear unable to satisfactorily constrain the coronal abundance, with any value larger than 0.1 times the solar value being acceptable at the 1σ level. As discussed below, the PSPC data do not provide an upper bound to the coronal abundance.

We have therefore fixed the coronal abundance, for the analysis of the PSPC data, to the value derived from the fit to the ASCA data, i.e. 0.9 times the solar value (compatible with the expected photospheric metallicity of HD 283572), still using the two-temperatures absorbed MEKAL model. In this case, the best-fit temperatures are 0.67 and 3.4 keV, with a ratio between the emission measures of 0.38. The X-ray luminosity, calculated in the 0.2–3.5 keV band, is 1.0×10^{31} erg s⁻¹, and the emission measures for the cool and hot component are 1.65×10^{53} cm⁻³ and 4.36×10^{53} cm⁻³. The best-fit absorbing column density is lower than in the case of the ASCA spectrum, at 0.4×10^{21} cm⁻², and thus very similar to the optically-derived value, but however again with ample confidence regions which include the ASCA best-fit value. The reduced χ^2 of the fit is 0.76, with 14 degrees of freedom, implying a probability of 70%

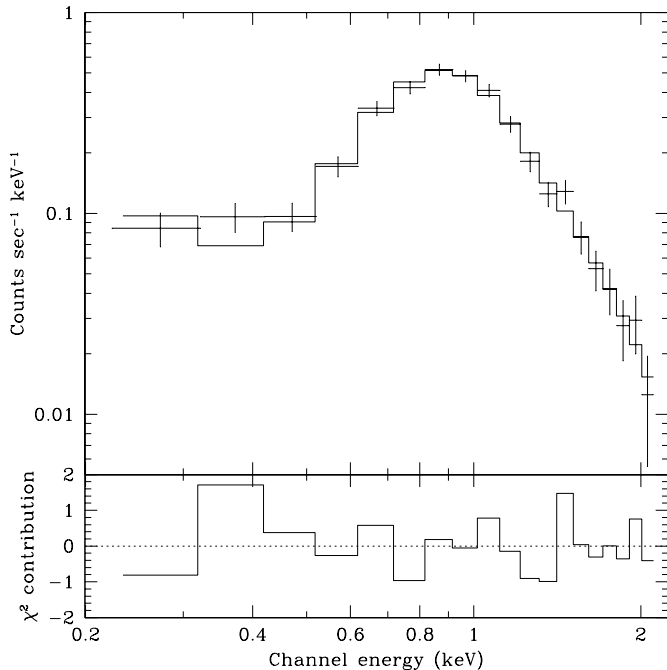


Fig. 5. Spectral fitting of the PSPC data. The top panel shows the background-subtracted spectrum, rebinned to have at least 20 counts per (variable-size) bin, plotted together with the best-fit two-temperature MEKAL model with an absorbing column density, while the bottom panel shows the (signed) contribution of each bin to the total χ^2 .

that the model is consistent with the data. The spectrum and the best-fit model are shown in Fig. 5.

3.3.3. Spectral fitting, SAX data

The SAX LECS and MECS spectra were fit simultaneously, again with an absorbed two-temperature collisional equilibrium of ionization model, as done for the ASCA data. The spectra were fit from 0.1 to 6.0 keV for the LECS data and from 1.6 to 9.0 keV for the MECS data. The two-temperature model gives a good description of the data, with temperatures of 0.90 and 3.5 keV and emission measures of $6.94 \times 10^{53} \text{ cm}^{-3}$ and $8.18 \times 10^{53} \text{ cm}^{-3}$. The best-fit metallicity, at $0.34 Z_{\odot}$ is lower than the one for the ASCA spectrum, although the 1σ confidence regions overlap (see below). The best-fit column density is $2.2 \times 10^{21} \text{ cm}^{-2}$, similar to the ASCA-derived value (but however very ill-constrained), and the reduced χ^2 is fully acceptable, at 0.77 with 145 degrees of freedom, implying a probability that the model is consistent with the data of 98%. The X-ray luminosity in the 0.2–10. keV band implied by the best-fit model spectrum, at the Hipparcos distance, is $2.0 \times 10^{31} \text{ erg s}^{-1}$ (or $1.71 \times 10^{31} \text{ erg s}^{-1}$ in the 0.2–3.5 keV band), close to the X-ray luminosity at the time of the *Einstein* observation 16.5 yr earlier. The SAX spectra, together with the best-fit two-temperature model, are shown in Fig. 6.

If the ASCA best-fit temperatures and abundance are imposed onto the SAX spectra, a satisfactory fit can still be

found (as plausible given the overlapping 1σ confidence regions shown later), however the higher metal abundance of ASCA spectrum visibly over-predicts the Fe K line visible in the SAX MECS spectrum.

The Fe K line visible in the SAX spectrum confirms that the harder part of the X-ray spectrum of HD 283572 is fully thermal in nature, and incompatible with alternative explanation based on non-thermal mechanisms such as bremsstrahlung radiation. No Fe K line is clearly visible in the SIS spectrum. However, given both the shorter effective exposure time and the smaller effective area of the SIS at the energy of the Fe K line (about one third of the effective area of the combined SAX MECS detectors), the SAX MECS spectrum has a number of counts at Fe K which is about 10 times higher than for the SIS spectrum. We have verified that a line with the same equivalent width as the one observed in the MECS spectrum would be washed out by the rebinning process in the case of the SIS spectrum, showing that no incompatibility exists between the two.

We have also separately analyzed the MECS merged spectrum of the flare. The count rate of the source is, even during the flare, small, and therefore the MECS flare spectrum only has $\simeq 500$ counts (versus the $\simeq 5000$ counts of the out-of-flare spectrum), insufficient for a detailed spectral analysis. Exclusion of the flare spectrum from the complete SAX data-set does not alter the best-fit spectral parameters significantly. In particular the temperature of the hot component and the visible presence of the Fe K line are not driven by the presence of the flare.

A simple unabsorbed single-temperature MEKAL model supplies a satisfactory description of both the flare and out-of-flare MECS spectra in the interval between 1.5 and 8.0 keV, with the MECS flare spectrum showing evidence for a higher characteristic temperature than the out-of flare spectrum. The best-fit flare temperature is 4.0 keV, with a 90% confidence range of 3.2–5.1 keV, significantly higher than the values determined for the out-of-flare MECS spectrum, which has a best-fit temperature of 2.4 keV and a 90% confidence range of 2.3–2.6 keV.

3.3.4. Solution uniqueness

To determine the errors in the best-fit parameters of each spectrum we have studied the confidence regions for the various fits by the usual approach of χ^2 contouring. Following the formulation of Avni (1976), we assume three interesting parameters (i.e. the two coronal temperature and the metallicity), so that the 68, 90 and 99% confidence level on the best-fit parameters translate into $\Delta\chi^2 = [3.50, 6.25, 11.30]$.

The two-temperature fit to the ASCA SIS data produces a rather shallow χ^2 landscape, specially along the abundance axis. As shown in Fig. 7, the abundance is rather ill-determined with the 90% contour extending from $\simeq 0.1$ up to $\simeq 2$ times the solar value. A second minimum in χ^2 -space is also present at low abundance, implying however an unphysically high coronal temperature of $\gtrsim 10$ keV. In essence, the SIS spectra are, at this relatively low signal-to-noise ratio, unable to significantly constrain the metal abundance of the plasma.

Table 2. The best-fit spectral parameters for the ASCA, ROSAT and SAX X-ray spectra of HD 283572 discussed in the text. The emission measures are computed for the Hipparcos-derived distance of 128 pc. The metallicity was fixed, for the PSPC two-temperature fit, to the best-fit value from the ASCA SIS data. The first row reports, for ease of comparison, the spectral parameters derived by Walter et al. (1987) for the *Einstein* IPC observation using REV0-processed data; the coronal temperature found by Damiani et al. (1996) on the REV1 IPC data is, at 1.5 keV, very similar. X-ray luminosities are given in the 0.2–4.0 keV band (except for the *Einstein* IPC one, originally in the 0.1–4.1 keV band).

Instrument	T_1 keV	T_2 keV	EM_1 10^{53} cm^{-3}	EM_2 10^{53} cm^{-3}	Z	$N(\text{H})$ 10^{21} cm^{-2}	χ^2	L_X $10^{31} \text{ erg s}^{-1}$
<i>Einstein</i> IPC	–	2.2	–	50.00	1.00	1.0	–	2.1
ASCA SIS	0.88	2.5	1.21	5.35	0.90	1.4	0.81	0.8
ROSAT PSPC	0.67	3.4	1.65	4.36	0.90	0.4	0.76	1.0
SAX LECS+MECS	0.90	3.5	6.94	8.18	0.34	2.2	0.75	1.7

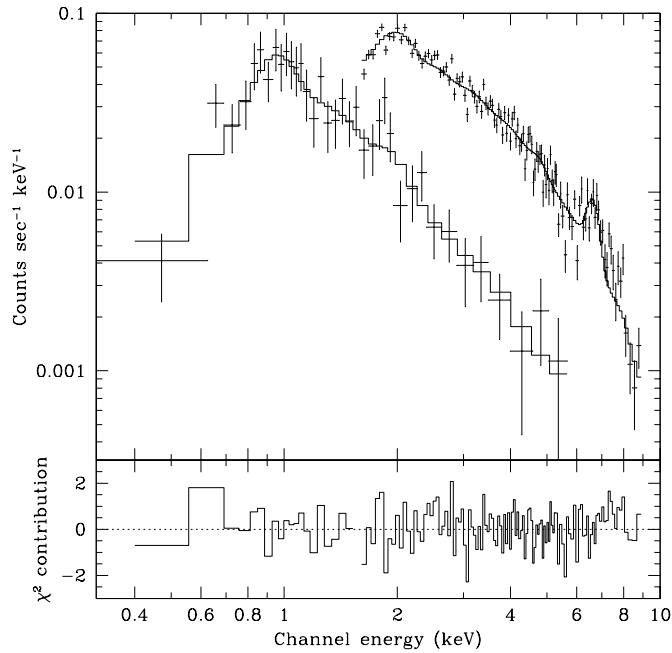


Fig. 6. Spectral fitting of the SAX data. The top panel shows the background-subtracted LECS spectrum and the merged spectrum from the three MECS detectors (shifted upwards by a factor of 2 for clarity), rebinned to have at least 20 counts per (variable-size) bin, plotted together with the best-fit two-temperature MEKAL model with an absorbing column density, while the bottom panel shows the (signed) contribution of each bin to the total χ^2 . These are shown for the LECS up to 1.5 keV and for the MECS for higher energies.

For the fit to the PSPC spectrum we have determined (not shown) the confidence regions for the coronal abundance and the absorbing column density obtained for a fit in which the best-fit metallicity is also left free to vary. They show that the PSPC is unable to effectively constrain the metallicity, with confidence regions which are open toward high metallicity values, thus justifying our choice, in the final fit to the PSPC spectrum, to freeze the metallicity to the best-fit value derived from the analysis of the ASCA SIS spectrum. Also, the confidence regions for the

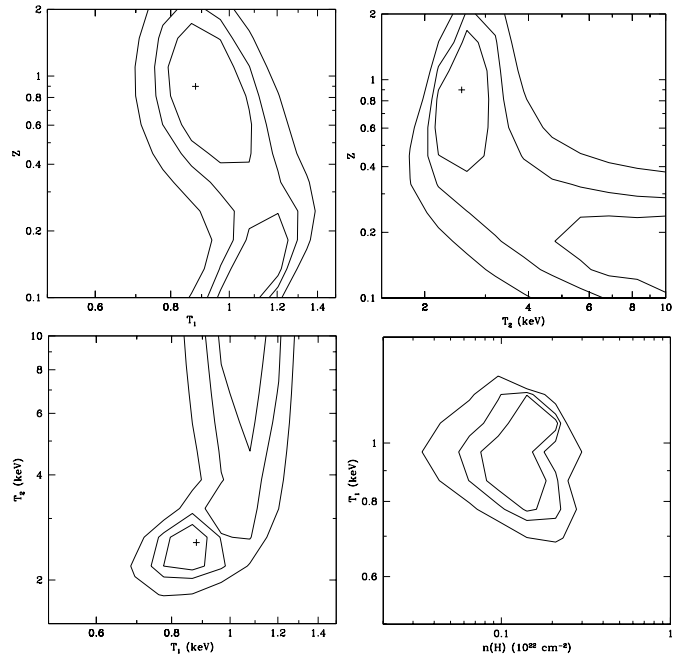


Fig. 7. χ^2 contour level plot for the two-temperature fit to the ASCA SIS spectrum. The χ^2 contours are shown as a function of the cool temperature T_1 and the global abundance Z (top left panel), of the two temperatures (bottom left panel), of the hot temperature T_2 and the global abundance Z (top right panel) and of the absorbing column density $N(\text{H})$ and the cool temperature T_1 (bottom right panel). The plotted contours are at $\Delta\chi^2 = [3.50, 6.25, 11.30]$, corresponding to probability levels of 68, 90 and 99% for three interesting parameters (Avni 1976).

two temperatures for the fit with fixed metal abundance shows that the PSPC spectrum is unable (because of its small passband) to effectively constrain the temperature of the hot component.

For the fit to the SAX LECS and MECS data the confidence regions (for the same set of parameters as for the fit to the SIS data) are shown in Fig. 8. The results of the fit to the SAX spectra are somewhat complementary to the ones obtained for the SIS data, as the shape of the confidence regions shows that the abundance and the temperature of the hot component are better

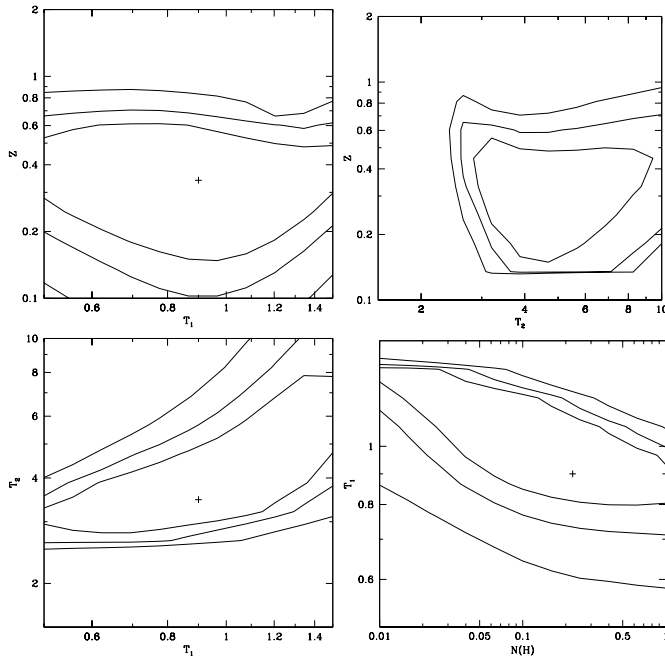


Fig. 8. χ^2 contour level plot for the two-temperature fit to the SAX LECS and MECS spectra. The χ^2 contours are shown as a function of the cool temperature T_1 and the global abundance Z (top left panel), of the two temperatures (bottom left panel), of the hot temperature T_2 and the global abundance Z (top right panel) and of the absorbing column density $N(\text{H})$ and the cool temperature T_1 (bottom right panel). The plotted contours are at $\Delta\chi^2 = [3.50, 6.25, 11.30]$, corresponding to probability levels of 68, 90 and 99% for three interesting parameters (Avni 1976).

constrained by the SAX spectra, while the temperature of the cooler component is better determined from the ASCA spectra (in agreement with the simulation shown by Favata et al. 1997). The difference in X-ray emission level between the ASCA and SAX observations is such that a joint analysis is unlikely to give a set of physically meaningful, better constrained spectral parameters. However, if we were to assume that the abundance is a “constant” in the quiescent corona, then the overlapping of the confidence regions supplies a value of $Z \sim 0.4 Z_\odot$.

3.3.5. Power-law temperature distributions

Power-law distributions of temperatures have at times been used in the literature to fit coronal X-ray spectra, on the assumption that the underlying continuous distribution of plasma temperatures would be better approximated as a power-law than as two discrete temperature components. In many cases such power-law distributions yield good fits to PSPC spectra (Preibisch 1997). We have thus also fit all the X-ray spectra discussed here with a continuous emission-measure distribution, assuming a power-law dependence with a cut-off at the hot end but no cut-off at the cool end, still using the same plasma emission model as in the two-temperature case. For this we have used the CEMEKL model in XSPEC. While a power-law emis-

sion measure supplies a satisfactory fit to the PSPC and SAX spectra, it does not yield a satisfactory fit to the SIS spectrum.

When the PSPC spectrum is fit with a power-law emission-measure distribution (again with the coronal abundance fixed to the ASCA-derived best-fit value), it yields a fully acceptable χ^2 , at 1.16 over 15 degrees of freedom. The power-law index is rather shallow, at 0.91, and the maximum temperature is 3.4 keV.

A power-law distribution of temperatures also supplies a satisfactory a fit to the SAX data, with a reduced χ^2 of 0.77. In this case the slope of the power-law is 1.58, with a maximum temperature of 3.63 keV, and a best-fit metal abundance of $0.53 Z_\odot$.

Power-law distributions of temperature do not however supply a good description to the SIS data: the best fitting model in this case has a reduced χ^2 of 1.23, significantly worse than the one obtained with the two-temperature model. The best-fit parameters for the SIS spectrum are rather similar to the ones obtained with the power-law emission measure model with the PSPC spectrum, with a shallow slope for the power-law of $\simeq 1.1$ and a maximum temperature of $\simeq 3.4$ keV. The χ^2 space for the power-law emission model is however very shallow, so that several rather equivalent solutions exist.

4. Discussion

The derived X-ray luminosity of HD 283572 is rather similar to the values observed in PMS stars in the ρ Oph and Cha I star-forming regions (Preibisch 1997), which have similar estimated ages, thus supporting the view of HD 283572 as a typical PMS X-ray source. It can therefore serve as prototype to interpret the observations of X-ray sources in star-forming regions at larger distances, for which detailed X-ray spectroscopy is not possible. It is well known that the dominant X-ray temperatures in a corona increase with increasing X-ray luminosity (Vaiana 1983). HD 283572 is no exception to this rule, with both the ASCA and SAX data showing that the dominant plasma is at temperatures of $\simeq 3$ keV, higher than the temperatures observed in less active single stars. Also, the presence of significant local absorption is evident, with derived values of the absorbing column density compatible with the ones derived from the optical spectrum of HD 283572.

The confidence regions of the fits to the ASCA and SAX spectra show a rather different shape, and cover different regions in parameter space, with the SAX data favouring a lower value of the coronal metallicity and the ASCA data compatible with a photospheric value. The confidence regions however overlap at the 1σ level, showing that no discrepancy is present from a statistical point of view. The overlap region favours a value of $Z \sim 0.4 Z_\odot$. While no determinations of the photospheric abundance exist in the literature for HD 283572, this value is lower than the solar photospheric abundance values which have been determined (Padgett 1996) through high-resolution spectroscopy on other members of the Tau-Aur star-forming region.

The temporal span of the X-ray observations discussed here is 16.5 years, although with a rather uneven coverage. This long time span allows us to discuss both the long- and short-term

X-ray variability of HD 283572. The average values listed in Table 2 for each observations show that the X-ray luminosity of HD 283572 in the 0.2–4.0 keV band is variable, with a peak-to-peak amplitude of a factor of 2.6. This is similar to the level of the short-term variability observed in each individual observation on time scale of the order of tens of kiloseconds. In addition, the SAX observation shows the presence of a short lived flare, with an enhancement in count rate of a factor of 4. The statistics and the temporal coverage do not allow for a determination of the flare decay time scale, however it is possible to show that the count-rate has returned to the pre-flare value in the satellite orbit following the one in which the flare is visible, i.e. ~ 5 ks later.

Acknowledgements. This paper made use of the services of the HEASARC and SAX-SDC data archives. The BeppoSAX satellite is a joint Italian and Dutch program. We thanks F. Reale for his careful reading of the manuscript and for the several useful suggestions.

References

- Avni Y. 1976, ApJ 210, 642
Damiani F., Micela G., Sciortino S., Harnden, F. R. J. 1995, ApJ 446, 331
Favata F., Maggio A., Peres G., Sciortino S. 1997, A&A 326, 1013
Favata F., Micela G., Sciortino S., D'Antona F. 1998, A&A in press
Gehrels N. 1986, ApJ 303, 336
Joncour I., Bertout C., Bouvier J. 1994, A&A 291, L19
Mewe R., Kaastra J. S., Liedahl D. A. 1995, Legacy 6, 16
Morrison R., McCammon D. 1983, ApJ 270, 119
Padgett D. L. 1996, ApJ 471, 847
Preibisch T. 1997, A&A 320, 525
Schrijver C. J., Mewe R., Walter F. M. 1984, A&A 138, 258
Strom K. M., Strom S. E., Edwards S., Cabrit S., Skrutskie M. F. 1989, AJ 97, 1451
Vaiana G. S. 1983, in J. O. Stenflo (ed.), Solar and Stellar Magnetic Fields: Origins and Coronal Effects, Reidel, p. 165
Walter F. M., Brown A., Linsky J. L. et al. 1987, ApJ 314, 297